

Structural relaxation in a system of dumbbell molecules

S.-H. Chong and W. Gotze

Physik-Department, Technische Universität München, 85747 Garching, Germany

(Dated: April 14, 2024, Phys. Rev. E, in press)

The interaction-site-density-fluctuation correlators, the dipole-relaxation functions, and the mean-squared displacements of a system of symmetric dumbbells of fused hard spheres are calculated for two representative elongations of the molecules within the mode-coupling theory for the evolution of glassy dynamics. For large elongations, universal relaxation laws for states near the glass transition are valid for parameters and time intervals similar to the ones found for the hard-sphere system. Rotation-translation coupling leads to an enlarged crossover interval for the mean-squared displacement of the constituent atoms between the end of the von Schweidler regime and the beginning of the diffusion process. For small elongations, the superposition principle for the reorientational process is violated for parameters and time intervals of interest for data analysis, and there is a strong breaking of the coupling of the relaxation scale for the diffusion process with that for representative density fluctuations and for dipole reorientations.

PACS numbers: 64.70.Pf, 61.20.Lc, 61.25.Em

I. INTRODUCTION

Recently, the mode-coupling theory (MCT) for the evolution of glassy dynamics in systems of spherical particles has been extended to a theory for systems of molecules. The fluctuations of the interaction-site densities have been used as the basic variables to describe the structure of the system. As a result, the known scalar MCT equations for the density fluctuations in simple systems have been generalized to n -by- n matrix equations for the interaction-site-density correlators, where n denotes the number of atoms forming the molecule. The theory was applied to calculate the liquid-glass phase diagram and to evaluate the glass-form factors for a hard-dumbbell system (HDS) [1]. In the following, the preceding work shall be continued by evaluating the conventional time-dependent correlation functions near the liquid-glass transition. It is the goal to examine the range of validity of the universal relaxation laws and to identify features of the glassy dynamics which are characteristic for molecular as opposed to atomic systems.

The dumbbells to be studied consist of two equal hard spheres of diameter d which are fused so that there is a distance $d, 0 < d < 1$, between their centers. The system's equilibrium structure for density is specified by two control parameters: the elongation parameter and the packing fraction $\phi = \frac{\pi}{6} d^3 (1 + \frac{3}{2} \frac{d}{2} - \frac{1}{2} d^3)$. The liquid-glass transition points $\phi_c(d)$ form a non-monotonic $\phi_c(d)$ versus d curve in the ϕ - d control-parameter plane with a maximum for d near 0.43. There is a second transition line $\phi_A(d)$ within the glass phase $\phi > \phi_c(d)$. It separates a plastic-glass phase for $\phi_c(d) < \phi < \phi_A(d)$, where dipole motion is ergodic, from a glass for $\phi > \phi_A(d)$, where also the molecular axes are arrested in a disordered array. The second line $\phi_A(d)$ terminates at $\phi_c = 0.345$, where $\phi_A(\phi_c) = \phi_c(\phi_c)$ (cf. Fig. 1 of Ref. 1). In the present paper, it shall be shown that there are two scenarios for the liquid-glass transition dynamics for $d > \phi_c$. The first one, to be demonstrated for

$d = 1.0$, deals with strong steric hindrance for reorientational motion. For this case, all universal relaxation laws hold within similar parameters and time intervals as found for the hard-sphere system (HSS) [2, 3]. As a new feature, there appears a very large crossover interval for the process of the constituent atoms' mean-squared displacement for times between the end of von Schweidler's power law and the beginning of the diffusion regime. The other scenario, to be shown for $d = 0.4$, deals with weak steric hindrance for reorientational motion. The universal laws for the reorientational process are restricted to such narrow $\phi_c(d)$ intervals that they are practically irrelevant for the interpretation of data obtained by molecular-dynamics simulations or by presently used spectrometers.

The paper is organized as follows. In Sec. IIA, the MCT equations of motion for the coherent and incoherent density correlation functions for the HDS are listed. Section IIB contains known universal laws for the MCT glass transition. The next section presents the new results for representative density-fluctuation correlators (Sec. IIIC), for the dipole dynamics (Sec. IIIB), for the mean-squared displacements (Sec. IIIC), and for the relaxation scales (Sec. IIID). The findings are summarized in Sec. IV.

II. MCT EQUATIONS FOR THE HDS

A. Equations of motion for the density correlators

In this subsection, the basic equations for the system of symmetric hard dumbbells are noted. They have been derived in Ref. 1, and their solutions underlie all results to be discussed in the present paper.

If \mathbf{r}_i^a , $a = A$ or B , denote the interaction-site centers of the i th AB dumbbell molecule, the interaction-site-density fluctuations for wave vector \mathbf{q} read $\delta \rho_{\mathbf{q}}^a = \frac{1}{N} \sum_i \exp(i\mathbf{q} \cdot \mathbf{r}_i^a)$. Similarly, the tagged-molecule-density

uctuations read $\bar{a}_{q;s} = \exp(iq \cdot \bar{r}_s^a)$ with \bar{r}_s^a denoting the interaction-site positions of the tagged molecule. It is convenient to transform to total number densities $\bar{n}_q = (\bar{A}_q + \bar{B}_q)/2$ and "charge" densities $\bar{z}_q = (\bar{A}_q - \bar{B}_q)/2$. Similar definitions are used for the tagged-molecule densities. The top-down symmetry of the molecules implies vanishing cross correlations $h_q^N(t) \bar{z}_q(0) = h_{q;s}^N(t) \bar{z}_{q;s}(0) = 0$ and also the identity $h_q^Z(t) \bar{z}_q(0) = h_{q;s}^Z(t) \bar{z}_{q;s}(0) = h_{q;s}^Z(t) \bar{z}_{q;s}(0) = h_{q;s}^Z(t) \bar{z}_{q;s}(0)$. There is only one independent coherent density correlator, which shall be used as normalized function

$$\bar{n}_q(t) = h_q^N(t) \bar{n}_q(0) = h_{q;s}^N(t) \bar{n}_{q;s}(0) \quad (1)$$

There are two incoherent density correlators

$$\bar{x}_{q;s}(t) = h_{q;s}^x(t) \bar{x}_{q;s}(0) = h_{q;s}^x(t) \bar{x}_{q;s}(0) \quad x = N, Z \quad (2)$$

Because of rotational invariance, the density correlators depend on the wave-vector modulus $q = |q|$ only. The short-time asymptotics of the correlators read: $\bar{n}_q(t) = 1 - \frac{1}{2}(\bar{n}_q(t))^2 + O(t^3)$ and $\bar{x}_{q;s}(t) = 1 - \frac{1}{2}(\bar{x}_{q;s}(t))^2 + O(t^3)$. The characteristic frequencies are given by the formulas: $(\bar{n}_q)^2 = q^2 v_T^2 [1 + j_0(qd)] + (v_R^2 d^2 = 6) [1 - j_0(qd)]$ and $(\bar{x}_{q;s})^2 = q^2 v_T^2 [1 - j_0(qd)] + (v_R^2 d^2 = 6) [1 - j_0(qd)]$ for $x = N, Z$. Here j_ν denotes the spherical Bessel function for index ν , S_q^N abbreviates the total-density structure factor, and $w_q^x = 1 - j_0(qd)$ for $x = N, Z$ are the intramolecular structure factors. Furthermore, $v_T = \sqrt{k_B T / 2m}$ denotes the thermal velocity for translation of the molecule of atomic mass m at temperature T , and $v_R = (2d/v_T)$ is the thermal velocity for rotations. The Zwanzig-Mori equations of motion [4] for the specified correlation functions are:

$$\begin{aligned} \partial_t^2 \bar{n}_q(t) + \int_0^t \bar{n}_q(t-t') \bar{n}_q(t') dt' &= 0; \\ \partial_t^2 \bar{x}_{q;s}(t) + \int_0^t \bar{x}_{q;s}(t-t') \bar{x}_{q;s}(t') dt' &= 0; \end{aligned} \quad (3)$$

for $x = N, Z$. All complications of the dynamics of the many-particle problem are hidden in the relaxation kernels $\bar{n}_q(t)$ and $\bar{x}_{q;s}(t)$.

Within MCT, the relaxation kernel $\bar{n}_q(t)$ is expressed as functional of the density correlators:

$$\bar{n}_q(t) = F_q^N[\bar{n}(t)]: \quad (5a)$$

The mode-coupling functional reads $F_q^N[f] = \frac{1}{2} \int d\mathbf{k} V^N(\mathbf{q}; \mathbf{k}; \mathbf{p}) f_{\mathbf{k}} f_{\mathbf{p}}$ where $\mathbf{k} + \mathbf{p} = \mathbf{q}$, and the positive coupling vertices are given by the density, the structure factor S_q^N , and the direct correlation function c_q^N (cf. Eq. (20b) of Ref. 1). Wave-vector integrals are

converted into discrete sums by introducing some upper cutoff q and using a grid of M equally spaced values for the modulus: $qd = h=2; 3h=2; \dots; qh=2$. Thus, q can be considered as a label for an array of M values. Equation (3) then represents a set of M equations which are coupled by the polynomial

$$F_q^N[f] = \sum_{\mathbf{k}, \mathbf{p}} V_{q;\mathbf{k}, \mathbf{p}} f_{\mathbf{k}} f_{\mathbf{p}} \quad (5b)$$

It is an elementary task to express the M^3 positive coefficients $V_{q;\mathbf{k}, \mathbf{p}}$ in terms of the $V^N(\mathbf{q}; \mathbf{k}; \mathbf{p})$ (cf. Eq. (7) of Ref. 2). Similarly, one derives functionals for the kernels for the tagged-molecule functions:

$$\bar{x}_{q;s}^x = F_{q;s}^x[\bar{x}(t); \bar{n}(t)]; \quad x = N, Z \quad (6a)$$

Again, the functionals $F_{q;s}^x$ are given in terms of the equilibrium structure functions (cf. Eq. (23) of Ref. 1). After the discretization, the mode-coupling polynomial has the form

$$F_{q;s}^x[f_s^x; f] = \sum_{\mathbf{k}, \mathbf{p}} V_{q;\mathbf{k}, \mathbf{p}} f_{\mathbf{k};s}^x f_{\mathbf{p}}; \quad x = N, Z \quad (6b)$$

The following work is done for a cutoff $qd = 40$ and $M = 100$ wave-vector moduli. The structure factors are evaluated within the reference-interaction-site-model (RISM) theory [4, 5, 6]. In Ref. 1, the details of the static correlation functions have been discussed. Equations (3) and (5) are closed non-linear integro-differential equations to calculate the M correlators $\bar{n}_q(t)$. Using these correlators as input, Eqs. (4) and (6) are closed equations to evaluate the M correlators $\bar{x}_{q;s}(t)$ for $x = N$ and Z . The mathematical structure of Eqs. (3) and (5) is identical to that discussed earlier for the density correlators of the HSS [2]. The differences are merely the values of the frequencies \bar{n}_q and the values for the coupling constants $V_{q;\mathbf{k}, \mathbf{p}}$. A similar statement holds for Eqs. (4) and (6), which are the analogues of the equations for the motion of a sphere in the HSS [3]. Therefore, all general results discussed previously [2, 3] hold for the present theory as well.

In the rest of the paper, the diameter of the constituent atoms shall be chosen as unit of length, $d = 1$, and the unit of time is chosen so, that $v_T = 1$.

B. Universal laws

This subsection compiles the universal laws for the dynamics near the liquid-glass transition. They will be used in the following Sec. III to analyze the numerical solutions of the equations of motion. The derivation of these laws is discussed comprehensively in Refs. 2 and 3, where also the earlier literature on this subject is cited.

From the mode-coupling functional in Eq. (5b), one calculates an M -by- M matrix $C_{qk} = f \partial F_q^N[f] / \partial f_k^N = g(1 - f_k^N)^2$. Here $f_k^N = \bar{n}_k(t=1)$

denote the nonergodicity parameters for the density fluctuations of the glass states. This matrix has a non-degenerate maximum eigenvalue $E^c = 1$. The transition is characterized by $E^c = 1$. Here and in the following, the superscript c indicates that the quantity is evaluated for $\tau = \tau_c(\lambda)$. Let e and \hat{e} denote the right and left eigenvectors, respectively, at the critical points: $\sum_k C_{qk}^c e_k = e_q$, $\sum_q \hat{e}_q C_{qk}^c = \hat{e}_k$. The eigenvectors are fixed uniquely by requiring $e_q > 0$, $\hat{e}_q > 0$, $\sum_q \hat{e}_q e_q = 1$, and $\sum_q \hat{e}_q (1 - f_q^N) e_q = 1$. These eigenvectors are obtained as a byproduct of the numerical determination of $\tau_c(\lambda)$ described in Ref. 1. They are used to evaluate the critical amplitude

$$h_q^N = (1 - f_q^N)^2 e_q; \quad (7)$$

and the exponent parameter λ , $1=2 < \lambda$,

$$= \frac{1}{2} \sum_{q,k,p} \hat{e}_q f_q^N F_q^N [f^N] = \sum_k f_k^N \sum_p f_p^N g h_k^N h_p^N : \quad (8)$$

Furthermore, a smooth function of the control parameters λ and τ is defined by

$$= \sum_q \hat{e}_q f_q^N F_q^N [f^N] - F_q^N [f^N] g; \quad (9a)$$

In a leading expansion for small $\tau - \tau_c(\lambda)$, one can write

$$= C; \quad = (\tau - \tau_c(\lambda)) = \tau_c(\lambda); \quad (9b)$$

Glass states are characterized by $\lambda > 0$, liquid states by $\lambda < 0$, and $\lambda = 0$ specifies the transition. The nonergodicity parameter exhibits a square-root singularity. In a leading-order expansion for small λ , one gets

$$f_q^N = f_q^N + h_q^N \sqrt{1 - \lambda}; \quad \lambda > 0; \quad \lambda \leq 0: \quad (10)$$

At the transition, the correlator exhibits a power-law decay which is specified by the critical exponent a , $0 < a < 1=2$. In a leading-order expansion in $(1-\lambda)^a$, one gets

$$f_q^N(t) = f_q^N + h_q^N (t_0 - t)^a; \quad \lambda = 0; \quad (t - t_0) \rightarrow 1: \quad (11)$$

Here, t_0 is a time scale for the transient dynamics. The exponent a is determined from the equation $(1 - a)^2 = (1 - 2a) = \lambda$, where λ denotes the gamma function.

Let us consider the correlator $f_Y(t) = h_Y(t) Y(0) i = h_Y^j f_i$ of some variable Y coupling to the density fluctuations. Its nonergodicity parameter $f_Y = f_Y(t \rightarrow 1)$ obeys an equation analogous to Eq. (10): $f_Y = f_Y^c + h_Y \sqrt{1 - \lambda} + O(\lambda)$. The critical nonergodicity parameter $f_Y^c > 0$ and the critical amplitude $h_Y > 0$ are equilibrium quantities to be calculated from the relevant mode-coupling functionals at the critical point $\tau = \tau_c(\lambda)$. If $Y = x_{qjs}$, the correlator $f_Y(t)$ refers to the tagged-molecule-density fluctuations, $x_{qjs}^*(t)$. Their nonergodicity parameters $f_Y = f_{qjs}^x$ have

been discussed in Ref. 1, and the explicit formulas for the evaluation of $h_Y = h_{qjs}^x$ can be inferred from Ref. 3. For small values of λ , there is a large time interval, where $f_Y(t)$ is close to f_Y^c . Solving the equations of motion asymptotically for this plateau regime, one gets in leading order in the small quantities $f_Y(t) \rightarrow f_Y^c$ the factorization theorem:

$$f_Y(t) - f_Y^c = h_Y G(t); \quad (12)$$

The function $G(t)$ is the same for all variables Y . It describes the complete dependence on time and on control parameters via the first scaling law:

$$G(t) = \sqrt[p]{j - jg(t-t_0)}; \quad \lambda \geq 0: \quad (13)$$

Here

$$t - t_0 = j - j; \quad \lambda = 1=2a; \quad (14)$$

is the first critical time scale. The master functions $g(\hat{t})$ are determined by λ ; they can easily be evaluated numerically [7]. One gets $g(\hat{t} \rightarrow 0) = 1 - \hat{t}^a$, so that Eq. (11) for $Y = x_q$ is reproduced for fixed large t and λ tending to zero. Since $g(\hat{t} \rightarrow 1) = 1 - \sqrt[p]{1 - \lambda}$, also Eq. (10) is reproduced.

One finds for the large rescaled time \hat{t} : $g(\hat{t} \rightarrow 1) = B \hat{t}^b + O(1 - \hat{t}^b)$. The anomalous exponent b , $0 < b < 1$, which is called the von Schweidler exponent, is to be calculated from λ via the equation $(1 + b)^2 = (1 + 2b) = \lambda$. The constant B is of order unity, and is also fixed by [7]. Substituting this result into Eqs. (12) and (13), one obtains von Schweidler's law for the decay of the liquid correlator below the plateau f_Y^c :

$$f_Y(t) = f_Y^c - h_Y (t - t_0)^b; \quad t \rightarrow t_0; \quad \lambda \rightarrow 0: \quad (15)$$

The control parameter dependence is given via the second critical time scale t^0 :

$$t^0 = t_0 B^{1-b} = j - j; \quad \lambda = (1=2a) + (1=2b): \quad (16)$$

The leading corrections to the preceding formulas for fixed $\hat{t} = t - t_0$ are proportional to $j - j$. They are specified by two correction amplitudes and additional scaling functions $h(t - t_0)$ [2]. The dynamical process described by the cited results is called λ -process. The λ -correlator $G(t)$ describes in leading order the decay of the correlator towards the plateau value f_Y^c within the interval $t_0 - t \rightarrow t$. The glass correlators arrest at f_Y for $t \rightarrow t$. In the limit $\lambda \rightarrow 0$, all correlators cross their plateau f_Y^c at the same time t , given by

$$t = \hat{t} - t; \quad (17)$$

Here, the number \hat{t} is fixed by $g(\hat{t}) = 0$.

The decay of $f_Y(t)$ below the plateau f_Y^c is called the λ -process for variable Y . For this process, there holds the second scaling law in leading order for $\lambda \rightarrow 0$:

$$f_Y(t) = \tilde{f}_Y(\hat{t}); \quad \hat{t} = t - t^0; \quad t \rightarrow t; \quad (18)$$

which is also referred to as the superposition principle. The control-parameter-independent shape function $\tilde{\gamma}(\zeta)$ is to be evaluated from the mode-coupling functionals at the critical point. For short rescaled times ζ , one gets $\tilde{\gamma}(\zeta) = f_Y^c - h_Y \zeta^b + O(\zeta^{2b})$, so that Eq. (15) is reproduced. The ranges of applicability of the first and the second scaling laws overlap; both scaling laws yield von Schweidler's law for $\zeta \ll \zeta_c$.

The superposition principle implies coupling of the relaxation time scales or relaxation rates of all the variables in the following sense. Let us characterize the long-time decay of $\gamma_Y(t)$ in the liquid by some time τ_Y . For example, as is occasionally done in analyzing molecular-dynamics simulation data, it may be defined as the center of the process, i.e. as the time at which the correlator has decayed to 50% of its plateau value:

$$\gamma_Y(\tau_Y) = f_Y^c/2: \quad (19)$$

This time diverges upon approaching the glass transition: in the leading asymptotic limit for $\zeta \rightarrow 0$, one finds $\tau_Y = C_Y \tau^0$. Here, the constant C_Y is defined by $\tilde{\gamma}_Y(C_Y) = f_Y^c/2$. All times or rates are proportional to each other, and follow a power law specified by the exponent defined in Eq. (16):

$$1/\tau_Y = \tau_Y^{-1} = \tau_Y^{-1} j: \quad (20)$$

The constants of proportionality C_Y or τ_Y depend on the variable Y and on the precise convention for the definition of τ_Y , such as Eq. (19). All the time scales or rates are coupled in the sense that the ratio $C_Y = C_{Y^0}$ or $\tau_Y = \tau_{Y^0}$ for two different variables Y and Y^0 becomes independent of the control parameters in the limit $\zeta \rightarrow 0$.

Figure 1 shows that for large elongations, say $\zeta > 0.6$, and for very small elongations, say $\zeta < 0.2$, the exponent parameter α is close to the value 0.736 ± 0.003 for the HSS ($\zeta = 0$). For ζ_c , the two contributions to the structure-factor peak for angular-momentum indices $l = 0$ and $l = 2$ are of equal importance [1]. For such elongations, α increases considerably. Unfortunately, Eq. (8) is so involved that we cannot trace back the increase of α to the underlying variations of the structure factor.

The accurate determination of the time scale t_0 is cumbersome. It is given by the constant plateau value of the function $\langle \gamma_q(t) \rangle = f_q^c - h_q^c t^a$ within the time interval where the leading-order Eq. (11) is valid. The leading corrections to this law vary proportional to $(t/t_0)^{2a}$ and cause deviations from the plateau at small times. The unavoidable errors in the determination of the critical value $\zeta_c(\zeta)$ cause $\delta \neq 0$ in Eq. (9b). Thus, $\langle \gamma_q(t) \rangle$ increases proportional to t or t for $t \ll 1$ if $\zeta > 0$ or $\zeta < 0$, respectively. For example, to determine t_0 for $\zeta = 1.0$ with an error estimated to be smaller than 3%, we have fixed $\zeta_c(\zeta)$ with 9 relevant digits. The plateau regime of $\langle \gamma_q(t) \rangle$ is largest for $q = 9.8$, where $f_q^{N,c}$ has an intermediate value; it extends from $t = 10^4$ to $t = 10^9$. We have checked that results for $q = 3.0, 7.4, 13.0$, and

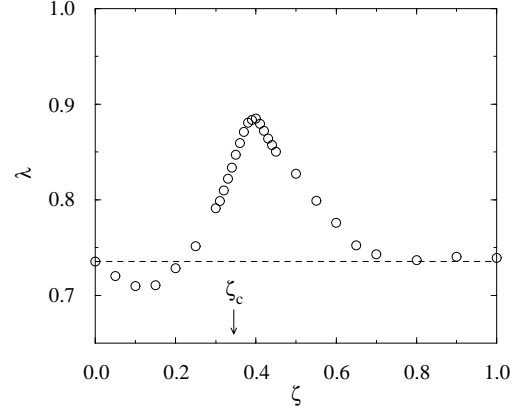


FIG. 1: Exponent parameter α as function of the elongation ζ . The arrow indicates the critical elongation $\zeta_c = 0.345$ separating the two glass phases. The dashed horizontal line marks the value $\alpha = 0.736$ for the hard-sphere system.

TABLE I: Parameters characterizing the MCT-liquid-glass-transition dynamics for systems with elongations $\zeta = 0.0, 0.4$, and 1.0 .

	ζ_c	C	t_0		a	b	B	\hat{t}	
0.0	0.530	1.54	0.0220	0.736	0.311	0.582	2.46	0.838	0.703
0.4	0.675	1.81	0.0123	0.885	0.222	0.330	3.77	2.54	0.110
1.0	0.565	1.90	0.0139	0.739	0.310	0.576	2.48	0.857	0.687

16.2 lead to the same t_0 within the specified error. A similar statement holds for the determination of t_0 for other elongations.

Table I compiles the parameters characterizing the universal formulas for the three elongations to be considered.

III. RESULTS FOR THE STRUCTURAL RELAXATION

A. Density correlators

Figures 2 and 3 demonstrate the coherent density correlators $\langle \gamma_q(t) \rangle$ and the tagged-molecule correlation functions $\langle \gamma_{q;s}^N(t) \rangle$ and $\langle \gamma_{q;s}^Z(t) \rangle$ near the liquid-glass transition for the elongations $\zeta = 0.4$ and 1.0 , respectively. The results are for two representative wave numbers q : the wave number $q = 7.0$ is close to the first peak, and $q = 9.8$ is near the first minimum of S_q^N (cf. Fig. 2 of Ref. 1). The oscillatory transient dynamics occurs within the short-time window $t < 1$. The control-parameter-sensitive glassy dynamics occurs for longer times for packing fractions ζ near ζ_c . At the transition point $\zeta = \zeta_c$, the correlators decrease in a stretched manner towards the plateau values ($f_q^{N,c}$, $f_{q;s}^{N,c}$ or $f_{q;s}^{Z,c}$) as shown by the dotted lines. Increasing ζ above ζ_c , the long-time limits increase, as shown for the coherent correlators $\langle \gamma_q(t) \rangle$ for $q = 9.8$. Decreasing ζ below ζ_c , the correlators cross

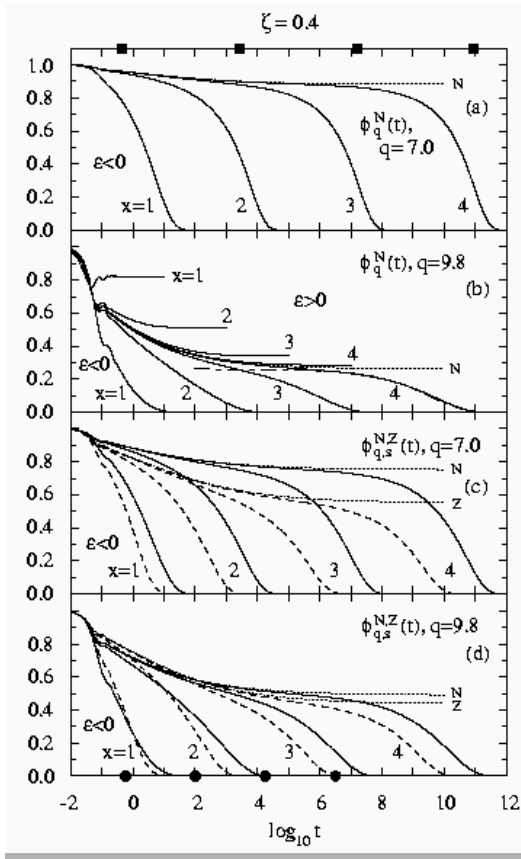


FIG. 2: Coherent density correlators $\phi_q^N(t)$ [solid lines in (a) and (b)], tagged-molecule density correlators $\phi_{q,s}^N(t)$ [solid lines in (c) and (d)], and tagged-molecule charge-density correlators $\phi_{q,s}^Z(t)$ [dashed lines in (c) and (d)] for the elongation $\zeta = 0.4$ as function of $\log_{10} t$ for two intermediate wave numbers $q = 7.0$ and 9.8 . The decay curves at the critical packing fraction ϕ_c are shown as dotted lines and marked by N and Z for the total density and charge density correlators, respectively. Glass curves ($\epsilon > 0$) are shown only for $\phi_q^N(t)$ with $q = 9.8$ in order to avoid overcrowding of the figure. The packing fractions are parameterized by $\phi = (\phi' - \phi_c)/\phi_c = 10^{-x}$, and $x = 1, 2, 3, 4$ are chosen. The dashed-dotted line in (b) is a Kohlrausch-law fit for the $x = 4$ process: $f_q^N \exp[-(t/t^0)^\beta]$ with $\beta = 0.40$. The filled circles and squares mark the characteristic times t^* and t^0 , respectively, defined in Eqs. (14) and (16) for $x = 1, 2, 3$ and 4 . Here and in the following figures, the diameter of the constituent atoms is chosen as the unit of length, $d = 1$, and the unit of time is chosen so that $v_T = 1$.

their plateaus at some time t^* , and then decay towards zero. For small $\phi' - \phi_c$, t^* is given by Eq. (17) for all the correlators. The decay from the plateau to zero is called the β -process. It is characterized, e.g., by the β -time scale defined as in Eq. (19) for each correlator. Thus, upon decreasing $\phi' - \phi_c$ towards zero, the time scales t^* and t^0 increase towards infinity proportional to t^* and t^0 , respectively. The two-step-relaxation scenario emerges, because the ratio of the scales t^0/t^* increases as well. Figures 2 and 3 exemplify the standard

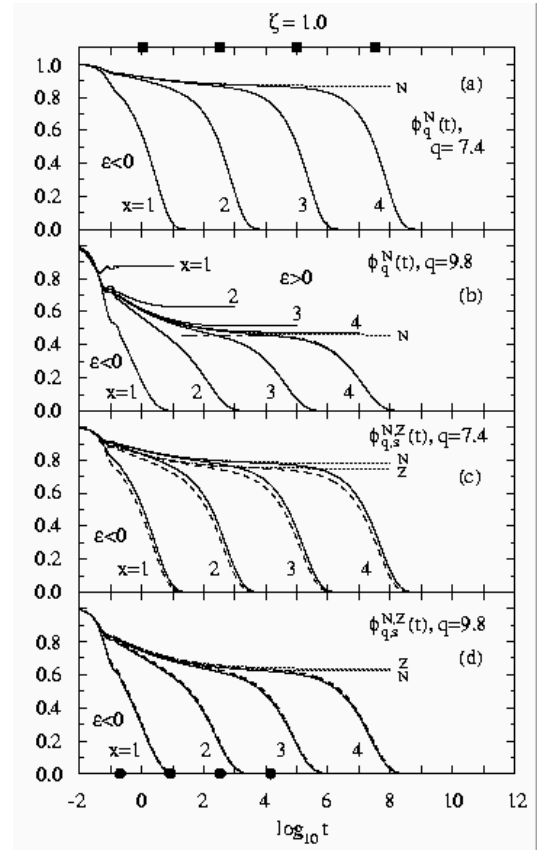


FIG. 3: Results as in Fig. 2, but for the elongation $\zeta = 1.0$ for wave numbers $q = 7.4$ and 9.8 , and a Kohlrausch exponent $\beta = 0.68$.

MCT-bifurcation scenario. For small $\phi' - \phi_c$, the results can be described in terms of scaling laws mentioned in Sec. II B. This was demonstrated comprehensively in Refs. 2 and 3 for the HSS, and the discussion shall not be repeated here.

For $\zeta = 1.0$ and $q \geq 5$, the plateaus for the tagged molecule's total-density and charge-density fluctuations are very close to each other: $f_{q,s}^{N,c} \approx f_{q,s}^{Z,c}$ (cf. Figs. 12 and 13 of Ref. 1). Figures 3(c) and 3(d) demonstrate that also the dynamics is nearly the same, $\phi_{q,s}^N(t) \approx \phi_{q,s}^Z(t)$. This means that for $q \geq 5$ and for strong steric hindrance, the cross correlations $F_{q,s}^{AB}(t)$ are very small. The reason is that the intramolecular correlation factors $j_\alpha(q, \alpha=2)$ are small, and thus interference effects between the density fluctuations of the two interaction sites are suppressed. Coherence effects can be expected only for small wave numbers. For this case, the functions can be understood in terms of their small- q asymptotes. The latter are determined by the dipole correlator and the mean-squared displacements [8], and their results shall be discussed in the following two subsections.

Figures 2(c) and 2(d) deal with tagged molecule's correlators of weak steric hindrance. In this case, the charge-density fluctuations behave quite differently from the total density fluctuations. The most important origin of

this difference is the reduction of the mode-coupling vertex in Eq. (6b) for $x = Z$ relative to the one for $x = N$. For small elongations, the effective potentials from the surroundings for the tagged molecule's reorientation are small. Therefore, $f_{q;s}^{Z,c}$ decreases strongly relative to $f_{q;s}^{N,c}$ for decreasing towards c (cf. Fig. 13 of Ref. 1). For

$c < c_c$, the charge-density fluctuations relax to zero as in a normal liquid. This implies, as precursor phenomenon, that the time scale $\tau_{q;s}^Z$ of the charge-density fluctuations shortens relative to the scale $\tau_{q;s}^N$ for the total density fluctuations. Thus, the differences between $N_{q;s}^N(t)$ and $N_{q;s}^Z(t)$ for small c shown in Figs. 2(c) and 2(d) are due to disturbances of the standard transition scenario by the nearby type-A transition from a normal glass to a plastic glass.

The stretching of the relaxation process is much more pronounced for the $c = 0.4$ system than for the $c = 1.0$ system. The wave vectors $q = 7.0$ and 7.4 refer to the structure-factor peak position for $c = 0.4$ and 1.0 , respectively, and the corresponding plateau values $f_q^{N,c}$ are almost the same. Figure 2(a) demonstrates that the $c = 0.4$ correlator for $c = 10^4$ requires a time increase by 2.3 decades for the decay from 90% to 10% of the plateau value $f_q^{N,c}$. The corresponding decay interval for the $c = 1.0$ correlator is 1.7 decades, as shown in Fig. 3(a). Thus, the specified time interval for the γ -process is 4 times larger for the small c than for the large elongation. Often, stretching is quantified by the exponent γ of the Kohlrausch-law fit for the γ -process: $\gamma(t) / \exp[-(t-t_0)^\gamma]$. Such fits are shown by the dashed-dotted lines for $N_q(t)$ for $q = 9.8$ and $c = 10^4$ in Figs. 2(b) and 3(b). For $c = 0.4$ and $c = 1.0$, the γ exponents are 0.40 and 0.68, respectively, quantifying the larger stretching for the smaller elongation. The transient dynamics for intermediate and large q is not very sensitive to changes of c . Both Figs. 2(b) and 3(b) for $q = 9.8$ demonstrate an initial decay of the correlators by about 20% if the time increases up to $t = 0.1$. This similarity is also reflected by the similarity of the microscopic time scale t_0 for the two elongations listed in Table I. However, for $c = 10^3$ or 10^4 , the correlators $N_{q;s}^N(t)$ require about 100 times longer times t for $c = 0.4$ than for $c = 1.0$ to decay to zero. All the enhanced stretching features reflect the fact that the anomalous exponents a and b are smaller for $c = 0.4$ than for $c = 1.0$ (cf. Table I).

A comment concerning the accuracy of the numerical solutions of the equations of motion might be in order. The primary work consists of calculating $N_q(t)$ from Eqs. (3) and (5) on a grid of times. In the work reported here, the initial part of the grid consists of 100 values with the equal step size $\Delta t = 10^{-5}$. This interval is then extended by successively doubling its length and the step size Δt . By inspection one checks $|j_{R,q}^N(t)| \leq 1$ so that the Laplace transform $N_q(z) = \int_0^\infty dt \exp(izt) N_q(t)$ exists as analytic function for $\text{Im } z > 0$. One checks for $c < 0$ that $N_q(t)$ decreases fast enough for large t so that $N_q(!) = \lim_{! \rightarrow 0} N_q(! + i) = N_q^0(!) + i N_q^{00}(!)$

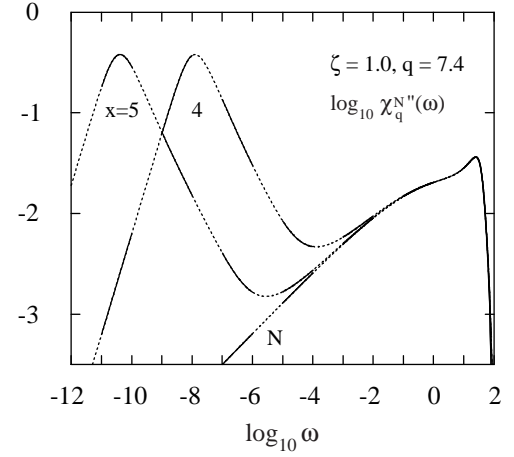


FIG. 4: Double logarithmic presentation of susceptibility spectra $N_q^{00}(!)$ as function of frequency $!$ for the density fluctuations discussed in Fig. 3(a) (see text).

exists with a smooth reactive part $N_q^0(!)$ and a smooth non-negative spectrum $N_q^{00}(!)$. The Fourier integrals are evaluated with a simplified Filon procedure [9]. The solid lines in Fig. 4 show results for the susceptibility spectrum $N_q^{00}(!) = ! N_q^{00}(!)$ for $c = 1.0$, $q = 7.4$, and $c = (f_c' / f_c) = f_c' / f_c = 10^x$ with $x = 4, 5$, and $x = 0$. The correlators are used to evaluate the polynomials $m_q^N(t) = \sum_{k,p} V_{q;kp} N_k(t) N_p(t)$ and from here one gets $m_q^N(!) = m_q^0(!) + i m_q^{00}(!)$. Equations (3) and (5) are solved if $N_q(!)$ agrees with $\tilde{N}_q(!) = 1/f! (N_q^0)^2 = [! + (N_q^0)^2 m_q^{00}(!)] g$. Because of causality, it suffices to check $\tilde{N}_q^{00}(!) = N_q^{00}(!)$. The functions $\tilde{N}_q^{00}(!)$ are shown as dotted lines in Fig. 4. The desired identity is verified by inspection within the accuracy better than that of the drawing. Corresponding statements hold for the other functions like $N_{q;s}^Z(t)$. The evaluation of $N_q(t)$ on the discrete set of times from Eqs. (3) and (5) is done by an extension of the method discussed in Ref. 10. But it should be noticed that the described proof of the accuracy of the solution does not require an account of how the solution $N_q(t)$ has been obtained.

B. Dipole correlators

The dipole correlator of the tagged molecule is defined by

$$C_{1;s}(t) = \langle \mathbf{e}_s(t) \cdot \mathbf{e}_s(0) \rangle \quad (21)$$

Here, the unit vector \mathbf{e}_s denotes the tagged molecule's axis. $C_{1;s}(t)$ is the reorientational-correlation function for angular-momentum index $l = 1$. For a similar reasoning as presented in the paragraph preceding Eq. (1), it is identical to the coherent reorientational function. It can be obtained as the zero-wave-vector limit of the

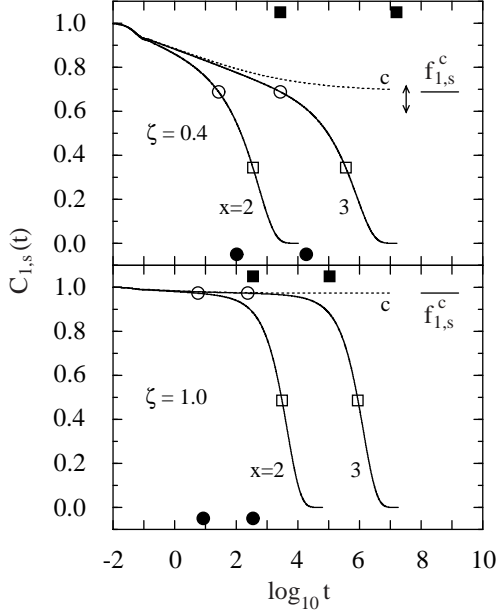


FIG. 5: Dipole correlators $C_{1;s}(t)$ for two elongations $\zeta = 0.4$ (upper panel) and 1.0 (lower panel). The correlators at the critical packing fraction $\phi = \phi_c$ are shown as dotted lines marked with c . The plateau $f_{1;s}^c$ for each elongation is marked by a horizontal line. The distance parameters are chosen as $\phi = (\phi - \phi_c)/\phi_c = 10^{-x}$ with $x = 2$ (faster decay) and $x = 3$ (slower decay). The filled circles and squares mark the corresponding time scales t^0 and t^1 , respectively, defined in Eqs. (14) and (16). The open circles and squares on the curves mark the characteristic time scales $t^{1;s}$ and $t^{0;s}$ defined by $C_{1;s}(t^{1;s}) = f_{1;s}^c$ and $C_{1;s}(t^{0;s}) = f_{1;s}^c/2$, respectively. The vertical line for $\zeta = 0.4$ indicates the decay interval described by the asymptotic formulas for the α -process (see text).

charge correlator: $\hat{C}_{q;s}^Z(t) = C_{1;s}(t) + O(q^2)$ [8]. $C_{1;s}(t)$ is evaluated most efficiently as follows. One carries out the $q \rightarrow 0$ limit in Eq. (4) for $x = Z$ to get the exact Zwanzig-Mori equation

$$\partial_t^2 C_{1;s}(t) + 2v_R^2 \partial_t C_{1;s}(t) + 2v_R^2 \int_0^t dt' m_s^Z(t-t') \partial_{t'} C_{1;s}(t') = 0; \quad (22)$$

to be solved with the initial condition $C_{1;s}(t) = 1 - (v_R t)^2 + O(t^3)$. The kernel is the $q \rightarrow 0$ limit of the relaxation kernel $m_{q;s}^Z(t)$ from Eqs. (6):

$$m_s^Z(t) = \left(\frac{2}{\pi} \right)^{1/2} \int_0^{2\pi} dk k^4 S_k^N (C_k^N)^2 w_k^Z C_{k;s}^Z(t) C_k^N(t); \quad (23)$$

The integral is discretized to a sum over M terms as explained in connection with Eq. (5b). Substituting the correlators $C_{k;s}^Z(t)$ and $C_k^N(t)$, the kernel $m_s^Z(t)$ is determined. The remaining linear integro-differential equation (22) is integrated to yield the desired result for $C_{1;s}(t)$. Equation (23) yields directly the nonergodicity

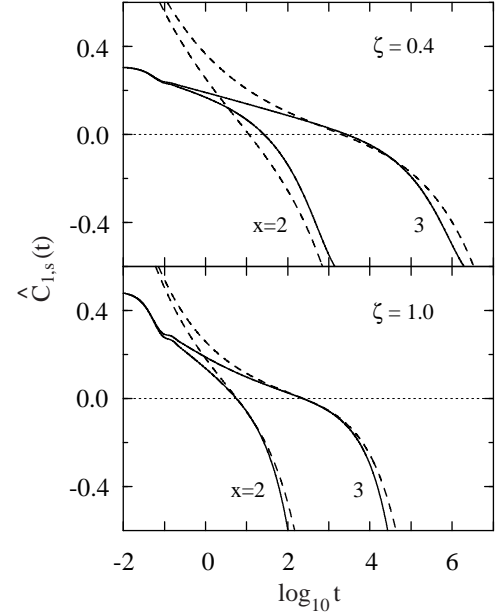


FIG. 6: Rescaled dipole correlators $\hat{C}_{1;s}(t) = [C_{1;s}(t) - f_{1;s}^c] / h_{1;s}$ (full lines) for two distance parameters $\phi = (\phi - \phi_c)/\phi_c = 10^{-x}$ with $x = 2$ (faster decay) and $x = 3$ (slower decay). The dashed lines show the α -correlators $G(t)$ from Eq. (13) for the exponents $\alpha = 0.885$ and 0.739 for the elongations $\zeta = 0.4$ and 1.0 , respectively (cf. Table I). Here $f_{1;s}^c = 0.69$ and 0.97 , and $h_{1;s} = 1.0$ and 0.056 for $\zeta = 0.4$ and 1.0 , respectively.

parameter of the kernel, $\hat{m}_s^Z = m_s^Z(t \rightarrow 1)$, as integral over the products of $f_{k;s}^Z f_k^N$. From \hat{m}_s^Z , one derives the probability for the arrest of the dipole $f_{1;s} = C_{1;s}(t \rightarrow 1) = \hat{m}_s^Z = (1 + \hat{m}_s^Z)$. This number can also be obtained as $f_{1;s} = \lim_{q \rightarrow 0} f_{q;s}^Z$. The critical value $f_{1;s}^c$ and the corresponding critical amplitude $h_{1;s} = \lim_{q \rightarrow 0} h_{q;s}^Z$ were discussed in Fig. 13 of Ref. 1.

The dipole correlators $C_{1;s}(t)$ for the elongations $\zeta = 0.4$ and 1.0 are shown in Fig. 5 for the critical point $\phi = \phi_c$ and for two liquid states. The time scales $t^{1;s}$ and $t^{0;s}$ characterizing the center of α - and β -relaxation processes, defined by $C_{1;s}(t^{1;s}) = f_{1;s}^c$ and $C_{1;s}(t^{0;s}) = f_{1;s}^c/2$, are marked by open circles and squares, respectively. The curves do not clearly exhibit the typical two-step-relaxation scenario. For $\zeta = 1.0$, the critical plateau is so large, $f_{1;s}^c = 0.97$, that only 3% of the decay are left for the transient motion and the critical relaxation. The results for $\zeta = 0.4$ are influenced by the nearby type-A transition. Let us consider the α -relaxation process for the dipole dynamics. The factorization theorem, Eq. (12), specializes to

$$C_{1;s}(t) = f_{1;s}^c + h_{1;s} G(t); \quad (24)$$

This means that the rescaled correlators $\hat{C}_{1;s}(t) = [C_{1;s}(t) - f_{1;s}^c] / h_{1;s}$ are given by the α -correlator $G(t)$. The latter obeys the scaling law, specified by Eq. (13)

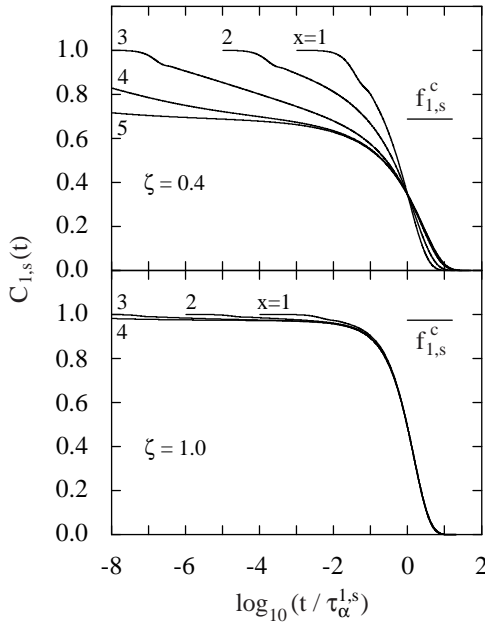


FIG. 7: Dipole correlators $C_{1,s}(t)$ for the elongations $\zeta = 0.4$ (upper panel) and 1.0 (lower panel) for various distance parameters $\beta = (\beta' - \beta_c) = 10^{-x}$ with x specified in the figure, presented as function of $\log_{10}(t/\tau_{\alpha}^{1,s})$. The τ -relaxation time scale $\tau^{1,s}$ is defined by $C_{1,s}(\tau^{1,s}) = f_{1,s}^c = 2$. The horizontal lines indicate the plateaus $f_{1,s}^c$.

and (14). For fixed rescaled time, $\hat{t} = t/\tau$, the cited formulas deal with the results correctly up to order β^{-1} . The leading corrections are of order β^{-2} , and they explain the range of validity of the leading results [2]. Figure 6 demonstrates the test of the τ -scaling law. On a 10% accuracy level, the leading-order asymptotic law accounts for 12% of the decay of $C_{1,s}(t)$ around the plateau for $\zeta = 0.4$, while it describes only 1.4% of the decay for $\zeta = 1.0$. The latter feature is due to the large critical nonergodicity parameter $f_{1,s}^c$, and hence, due to the small critical amplitude $h_{1,s}$, for the strong steric hindrance. The decay interval described by the leading-order asymptote for $\zeta = 0.4$ is indicated in Fig. 5 by the vertical line. For $\beta = 0.001$, the corresponding dynamical window extends from about $t = 1.1 \cdot 10^3$ to about $2.4 \cdot 10^4$, while it extends from about $t = 20$ to $t = 70$ for $\beta = 0.01$. This discussion requires a reservation. The corrections to the scaling results can lead to an offset of the plateau [2]. One recognizes that incorporation of such offset would improve the agreement between numerical solution and its asymptotic description in the upper panel of Fig. 6. The mentioned windows are obtained only after a plateau offset had been eliminated.

The τ -relaxation scaling law for the dipole correlator reads according to Eq. (18):

$$C_{1,s}(t) = \bar{C}_{1,s}(\hat{t}); \quad \hat{t} = t/\tau^0; \quad j \geq 1; \quad t \geq t_0 \quad (25)$$

The τ -independent master function $\bar{C}_{1,s}$ is determined

by the $q = 0$ limit of the mode-coupling functional $F_{q,s}^Z$ given in Eq. (6b) at the critical point. The τ -time scale $\tau^{1,s}$ can be defined by $C_{1,s}(\tau^{1,s}) = f_{1,s}^c = 2$, and shall be written as $\tau^{1,s} = \tau_{1,s}^0$. Here, the τ -scale factor $\tau_{1,s}^0$ is defined in terms of the master function as $\bar{C}_{1,s}(\tau_{1,s}^0) = f_{1,s}^c = 2$. The scaling law implies that a representation of $C_{1,s}(t)$ as a function of the rescaled time $\hat{t} = t/\tau^{1,s}$ should superimpose correlators for different distance parameters on the common curve $\bar{C}_{1,s}(\hat{t} = \tau_{1,s}^0)$. A symptotic validity means that the $\log(\hat{t} = \tau^{1,s})$ interval, where the scaling law is obeyed, expands to an arbitrary size for $\beta \rightarrow 0$.

The lower panel of Fig. 7 demonstrates that the described scenario for the evolution of the process is valid for the elongation $\zeta = 1.0$. On the other hand, the upper panel shows that the dipole correlators for $\zeta = 0.4$ exhibit the superposition principle only for $j \geq 10^4$. In particular, the plateau region emerges only for these extremely small values of the distance parameter $j \geq j_0$. As discussed in Ref. 2, this is because of the correction to the leading-order asymptotic law, which reads for not too large values of rescaled time \hat{t} :

$$C_{1,s}(t) = \bar{C}_{1,s}(\hat{t}) + j B_1 h_{1,s} \hat{t}^b; \quad (26)$$

with $B_1 = \frac{1}{2}[(1-b)(1+b)]$. Therefore, the correction is larger, the larger the product $B_1 h_{1,s}$ is. As discussed in connection with Fig. 13 of Ref. 1, the size of the critical amplitude $h_{1,s}$ becomes very large near the critical elongation ζ_c . In addition, B_1 increases with β . One gets $B_1 = 1.56$ and 0.45 for $\zeta = 0.4$ and 1.0 , respectively. Thus, the anomaly shown in the upper panel of Fig. 7 is due to the large correction to the leading-order asymptotic law, caused by the precursor effect of the nearby type-A transition and by the large value for β . The descriptions of correlators by the first and second scaling laws overlap for $t \geq t_0$. Therefore, the anomaly for $\zeta = 0.4$ exhibited in Fig. 7 can also be explained as the large percentage of the decay of $C_{1,s}(t)$ described by the τ -scaling law (cf. Fig. 5).

C. Mean-squared displacements

There are two mean-squared displacements (MSD) to be considered for the symmetric dumbbell. One refers to the position of the constituent atom of the tagged molecule \mathbf{r}_s^A , and the other to the molecule's center $\mathbf{r}_s^C = (\mathbf{r}_s^A + \mathbf{r}_s^B)/2$:

$$\Delta \mathbf{r}_s^C(t) = \langle [\mathbf{r}_s^A(t) - \mathbf{r}_s^A(0)]^2 \rangle = 6; \quad (27)$$

Here, a factor 6 is introduced in the definition for later convenience. Since there is the relation [8]

$$\Delta \mathbf{r}_s(t) = \Delta \mathbf{r}_s^C(t) + (\Delta \mathbf{r}_s^B(t) - \Delta \mathbf{r}_s^A(t)); \quad (28)$$

it is sufficient to calculate $\Delta \mathbf{r}_s^C(t)$. This function is determined by the small- q limit of the density correlator:

$f_{q;s}^N(t) = 1 - q^2 \langle c(t) \rangle + O(q^4)$ [8]. The small- q expansion of Eq. (4) for $x = N$ leads to the exact equation of motion

$$\partial_t^2 \langle c(t) \rangle = v_T^2 + v_T^2 \int_0^t dt' m_s^N(t-t') \partial_{t'} \langle c(t') \rangle = 0; \quad (29)$$

to be solved with the initial behavior $\langle c(t) \rangle = (1/2)(v_T t)^2 + O(t^3)$. The kernel is obtained as the $q \rightarrow 0$ limit of Eq. (6a) for $x = N$:

$$m_s^N(t) = \frac{1}{6} \int_0^t dk k^4 S_k^N (c_k^N)^2 w_k^N \frac{N}{k;s}(t) \frac{N}{k}(t); \quad (30)$$

After the discretization of the integrals as explained above and substituting the results for the two density correlators, the kernel $m_s^N(t)$ is determined. Then, the linear equation (29) is integrated to yield the MSD of the molecule's center.

The long-time behavior of the MSD depends sensitively on control parameters near the transition singularity, and therefore it is well suited to study the glass-transition precursors. In liquid states, one obtains from Eq. (29) the long-time asymptote: $\lim_{t \rightarrow \infty} \langle c(t) \rangle = D$. Here D is the diffusion constant, and it is expressed as the inverse of the zero-frequency spectrum of the relaxation kernel: $D = 1/\int_0^\infty dt m_s^N(t)$. In glass states, the tagged molecule's total density fluctuations arrest for long times: $f_{q;s}^N(t \rightarrow \infty) = f_{q;s}^N > 0$. The Lamb-Mössbauer factor $f_{q;s}^N$ approaches unity for q tending to zero, and a localization length, r_c , of the center characterizes the width of the $f_{q;s}^N$ versus q curve: $f_{q;s}^N = 1 - (qr_c)^2 + O(q^4)$. One gets $\lim_{t \rightarrow \infty} \langle c(t) \rangle = r_c^2$. Using Eq. (29), one can express r_c^2 as inverse of the long-time limit of the relaxation kernel from Eq. (30): $r_c^2 = 1/m_s^N(t \rightarrow \infty)$.

The ideal liquid-glass transition implies a transition from a regime with molecule's diffusion for $r_c < r_c^c$ to one with molecule's localization for $r_c > r_c^c$. The former is characterized by $D > 0$ and $1/r_c = 0$, and the latter by $D = 0$ and $1/r_c > 0$. The subtleties of the glass-transition dynamics occur outside the transient regime. Figure 8 exhibits the MSD of the molecule's center for various packing fractions near the transition. For very short times, say $t \ll t_0$, interaction effects are unimportant and $\lim_{t \rightarrow 0} \langle c(t) \rangle = t^2 = v_T^2/2$ reflects ballistic motion. For times larger than t_0 , the cage effect leads to a suppression of $\langle c(t) \rangle$ below the short-time asymptote. For long times in liquid states, the MSD approaches the diffusion asymptote, $\lim_{t \rightarrow \infty} \langle c(t) \rangle = D$, as shown by the dotted straight lines drawn for the curves with labels $x = 1$ and $x = 4$. Upon increasing r_c towards r_c^c , the diffusivity decreases towards zero.

The curves with $x = 1$ for $r_c > 0$ in Fig. 8 deal with the glass state $r_c = 1.1 r_c^c$. For this density, there is no obvious glassy dynamics. Rather, $\langle c(t) \rangle$ has approached its long-time limit r_c^2 after the oscillations have disappeared for $t \gg 1$. Decreasing r_c towards r_c^c , the softening of the glass manifests itself by an increase of the localization length r_c . At the transition point $r_c = r_c^c$, the

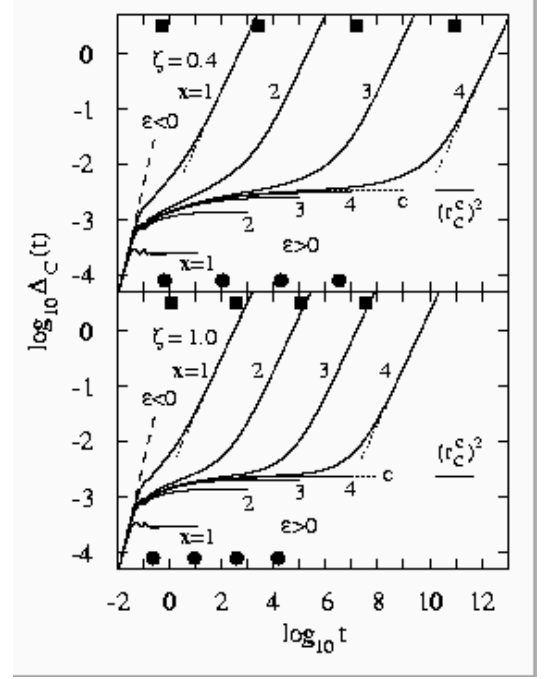


FIG. 8: Double logarithmic presentation of the mean-squared displacement for the center of mass $\langle c(t) \rangle$ for the elongations $\zeta = 0.4$ (upper panel) and 1.0 (lower panel). The dotted lines with label c refer to the critical packing fraction r_c^c , and the solid lines to $r_c = (r_c^c)^2 = 10^{-x}$ for $x = 1, 2, 3, 4$. The straight dashed line with slope 2 in each panel exhibits the ballistic asymptote $(v_T t)^2/2$. The straight dotted lines with slope 1 denote the long-time asymptotes D of the two liquid curves for $x = 1$ and $x = 4$. The horizontal lines mark the square of the critical localization lengths $(r_c^c)^2$. The filled circles and squares mark the characteristic times t^* and t^0 , respectively, defined in Eqs. (14) and (16) for $x = 1; 2; 3; 4$.

critical value $r_c^c = 0.0587$ (0.0497) for $\zeta = 0.4$ (1.0) is reached. Substituting Eq. (10) for $f_{q;s}^N$ and the analogous formula for $f_{q;s}^N$ to evaluate r_c^2 from Eq. (30), it follows that the glass instability at r_c^c causes a $\frac{1}{r_c^2}$ anomaly for the localization length,

$$r_c^2 = (r_c^c)^2 \left(\frac{h_c}{h_c^c} \right)^p \frac{1}{(1 - \frac{r_c^c}{r_c})} + O(\dots); \quad (31)$$

where $h_c = 9.66 \cdot 10^{-3}$ ($5.14 \cdot 10^{-3}$) for the elongation $\zeta = 0.4$ (1.0). A corresponding formula holds for the square of the localization length r_A for the constituent atom with $(r_c^c)^2$ replaced by $(r_A^c)^2 = (r_c^c)^2 + (\frac{1}{2} = 12)(1 - f_{1;s}^c)$ and h_c replaced by $h_A = h_c + (\frac{1}{2} = 12)h_{1;s}$ according to Eq. (28). In Fig. 9, the leading order results for r_c^2 and r_A^2 are shown as dashed and dotted lines, respectively. For $\zeta = 1.0$, the data are described by the square-root law for $r_c^2 \approx 2 \cdot 10^{-3}$. Similar small intervals for the validity of the leading order descriptions have been found for the Debye-Waller factor of the HSS for small wave vector q [2]. For $\zeta = 0.4$, the range of validity of the universal formula is reduced to the even smaller intervals $r_c^2 < 0.5 \cdot 10^{-3}$.

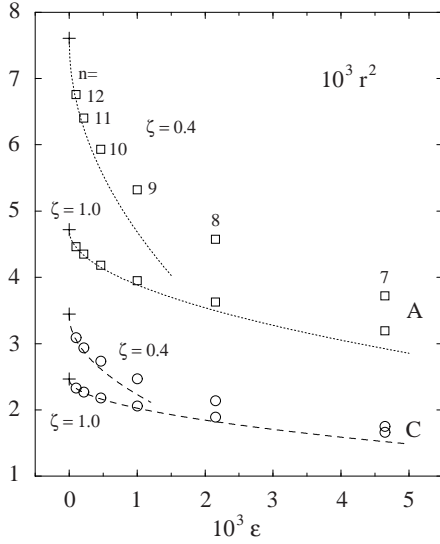


FIG. 9: Square of the localization lengths for the molecule's center r_c^2 (circles) and for the constituent atom r_A^2 (squares) for $\zeta = (\zeta_c) = \zeta_A = 10^{-n/3}$, $n = 7; 8; \dots; 12$. The crosses mark the critical values $(r_c^c)^2$ and $(r_A^c)^2$, respectively. The dashed and dotted lines are the leading order asymptotic laws $r_X^2 = (r_X^c)^2 + h_X (t-t^0)^{-1}$ for $X = C$ and A , respectively.

The glass curves for $\zeta = 0.01$, shown in Fig. 8 with label $x = 2$, exhibit a decay between the end of the transient oscillations and the arrest at r_c^2 which is stretched over a time interval of about two orders of magnitude. A similar two-decade interval is needed for the liquid curves ($\zeta < 0$) with label $x = 2$ to reach the critical value $(r_c^c)^2$. After crossing $(r_c^c)^2$, two further decades of an upward bent $\log_{10} r_c(t)$ versus $\log_{10} t$ variation is exhibited before the final diffusion asymptote is reached. The stretching is more enhanced as the system is driven towards the transition point, $j \rightarrow 1$. The indicated slow and stretched time variation outside the transient regime is the glassy dynamics exhibited by the MSD. Again, the stretching is more pronounced for $\zeta = 0.4$ than for $\zeta = 1.0$.

The first scaling law deals with the dynamics where $r_c(t) = (r_c^c)^2$ is small. One gets in analogy to Eqs. (12) and (13):

$$r_c(t) = (r_c^c)^2 + h_c \frac{t^p}{j} \quad (t \geq t^0); \quad p \geq 0; \quad (32)$$

for $j \rightarrow 1$ and $t \rightarrow t_0$. For glass states with $\zeta > 0$, this formula describes the approach towards the arrest at $r_c^2 = r_c(t \rightarrow 1)$. For liquid states with $\zeta < 0$, it describes how the $r_c(t)$ curve crosses and leaves the plateau $(r_c^c)^2$. In particular, one gets von Schweidler's law for large $t-t^0$ in analogy to Eq. (15):

$$r_c(t) = (r_c^c)^2 + h_c (t-t^0)^b; \quad b < 0; \quad t \rightarrow t^0; \quad (33)$$

The increase of $r_c(t)$ above the plateau towards the diffusion asymptote is the process of the MSD. In analogy

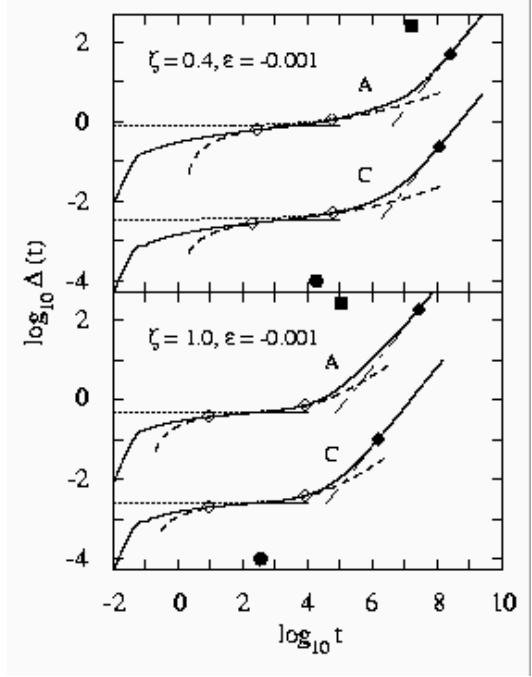


FIG. 10: Double logarithmic presentation of the mean-squared displacement for the constituent atom $r_A(t)$ and for the center $r_c(t)$ for the elongations $\zeta = 0.4$ (upper panel) and $\zeta = 1.0$ (lower panel). The curve $r_A(t)$ is shifted upwards by two decades to avoid overcrowding. The distance parameter is $\varepsilon = 10^{-3}$, and the corresponding times t^0 and t^1 are marked by filled circles and squares, respectively. The dashed lines are the first-scaling-law results, Eq. (32). The open diamonds mark the points where the dashed lines differ from the solid ones by 5%. The straight dashed-dotted lines exhibit the diffusion asymptotes $D t$, and the filled diamonds mark the position where these differ from the solid lines by 5%. The dotted lines exhibit the second-scaling-law results, Eq. (34). The horizontal lines mark the square of the localization lengths $(r_A^c)^2$ and $(r_c^c)^2$.

to Eq. (18), there holds the superposition principle

$$r_c(t) = \tilde{r}_c(\tilde{t}); \quad \tilde{t} = t-t^0; \quad j \rightarrow 1; \quad t \rightarrow t^0; \quad (34)$$

In Ref. 11, it has been discussed in detail how these leading-order asymptotic results can account quantitatively for the glassy dynamics of the MSD, albeit for the tagged spherical particle and the dumbbell molecule immersed in the hard-sphere system. Instead of repeating such an extensive analysis, we shall only show here some representative examples.

The upper and lower panels of Fig. 10, respectively for the elongations $\zeta = 0.4$ and 1.0 , exhibit such tests of the scaling-law descriptions for a liquid state which is sufficiently close to the transition point, $\zeta = 10^{-3}$. Also, the MSD of the constituent atom $r_A(t)$ is considered in these figures. Because of Eq. (28), the asymptotic laws (32) and (33) for $r_A(t)$ hold with $(r_c^c)^2$ replaced by $(r_A^c)^2 = (r_c^c)^2 + (\zeta^2=12)(1 - f_{1,S}^c)$ and h_c replaced by $h_A = h_c + (\zeta^2=12)h_{1,S}$. The range of validity of the

rst-scaling-law description is indicated by the open diamonds. One finds that such a range is nearly the same for both $r_C(t)$ and $r_A(t)$, and this holds irrespective of the molecule's elongation ζ . The beginning of the β -process of the MSD, i.e., its initial increase above the plateau, is described by von Schweidler's law, Eq. (33). It is exhibited for $t \ll t_c$ by the dashed lines. The β -process terminates in the diffusion law for long times, exhibited by the straight dashed-dotted lines. The beginning of the diffusion law is indicated by the filled diamonds for each MSD curve. The β -process follows well the second scaling law, Eq. (34), which is presented by the dotted lines. The descriptions by the two scaling laws overlap for $t \ll t_c$. Together, the two scaling laws provide a description of the glassy dynamics of the MSD for $t > 100$ and $t > 10$ for $\zeta = 0.4$ and $\zeta = 1.0$, respectively. Notice that there is a large interval of times outside the transient regime, say $\log_{10} t > 0.5$, where the structural relaxation is not described by the first scaling law. This is a peculiarity of the MSD [11] which is not found for the other functions discussed here.

The crossover window from the end of the von-Schweidler-law regime (indicated by the right open diamonds) to the beginning of the diffusion process (indicated by the filled diamonds) for the MSD of the center, $r_C(t)$, is about 3 (2) decades wide for $\zeta = 0.4$ (1.0). On the other hand, the corresponding window for the MSD of the constituent atom, $r_A(t)$, is larger than that of $r_C(t)$ by a factor of about 7 (13) for $\zeta = 0.4$ (1.0). As discussed in Ref. 11, this enlarged crossover window for $r_A(t)$ is caused by the rotation-translation coupling, i.e., by the second term on the right-hand side of Eq. (28). This effect is smaller for $\zeta = 0.4$ because the relaxation of the second term, determined by that of $C_{1;s}(t)$, is considerably enhanced due to the nearby type-A transition as discussed in connection with Fig. 5.

Figure 11 exhibits the critical localization lengths of the molecule's center r_C^c and of the constituent atom r_A^c as function of the elongation ζ . There are three distinct regions: one for small elongations, say $\zeta < 0.3$, another for large elongations, say $\zeta > 0.4$, and the crossover region between them. For $\zeta < \zeta_c$, the localization length of the center r_C^c is nearly constant while that of the constituent r_A^c increases rapidly with ζ . Both r_C^c and r_A^c decrease rapidly within the crossover region, and they decrease only slightly as function of the elongation for $\zeta > 0.4$. The rapid increase of r_A^c for $\zeta < \zeta_c$ can be understood as follows. Since $C_{1;s}(t \rightarrow 1) = 0$ for $\zeta > 1$, one gets from the long-time limit of Eq. (28): $r_A^c = \frac{\zeta}{(r_C^c)^2 + \zeta^2} = 12$. The dotted line in Fig. 11 shows this formula with r_C^c fixed to the value for $\zeta = 0.0$. It explains the increase of r_A^c for increasing up to ζ_c . Thus, r_A^c increases because the reorientational dynamics of the molecule's axis is not arrested for $\zeta < \zeta_c$. In this sense, the localization of molecules with small elongations is primarily caused by that of the molecule's center. This is consistent with the result that the glass transition for systems with small elongations is mainly driven by the

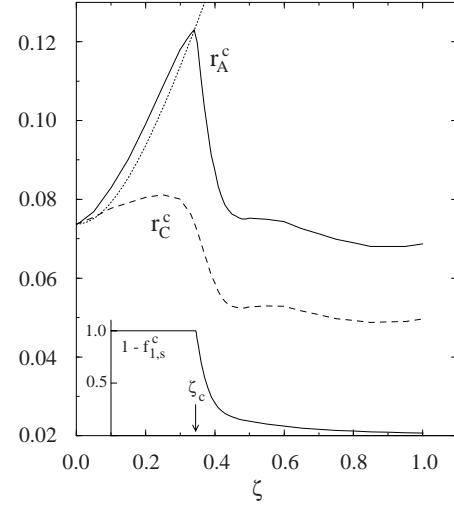


FIG. 11: Critical localization lengths for the constituent atom r_A^c (solid line) and the center r_C^c (dashed line) along the liquid-glass-transition line parameterized by the elongation ζ . The dotted line represents the function $\frac{1}{(r_C^c)^2 + \zeta^2} = 12$ discussed in the text. The inset exhibits $1 - f_{1;s}^c$ as function of ζ , where $f_{1;s}^c = C_{1;s}(t \rightarrow 1)$ is the long-time limit of the dipole correlator $C_{1;s}(t)$. The arrow indicates the critical elongation $\zeta_c = 0.345$.

arrest of the center-of-mass density fluctuations [1]. The critical localization length r_C^c provides the upper limit for r_C characterizing the size of the arrested structure, and its value $0.07 - 0.08$ for ζ_c is consistent with Lindemann's melting criterion. The critical localization length of the constituent atom r_A^c for $\zeta > 0.4$ has similar values. This implies that the localization of molecules with large elongations is caused by that of the molecule's constituents rather than by that of the molecule's center: the localization of the center is subordinate to that of the constituents. As explained in Ref. 1, angular correlations become more relevant for the glass transition of systems with large elongations. Such angular correlations result in more efficient localization of the constituent atoms, and this is the reason for the relevance of r_A^c for the localization of molecules with large elongations. The center localization is reduced by about $1/\sqrt{2}$, as expected for independent motion of the two constituents.

D. The β -relaxation scales

The superposition principles for various correlators imply coupling of the β -relaxation time scales or relaxation rates as described in Sec. IIB. This scale coupling or β -scale universality is demonstrated in Fig. 12 for the rate $1 = N$ of the coherent total density correlator $N_q(t)$ for the wave number $q \approx 7$, the rate $1 = 1/s$ of the dipole correlator $C_{1;s}(t)$, and the diffusion constant D . Here, the β -relaxation times for $N_q(t)$ and $C_{1;s}(t)$ are determined

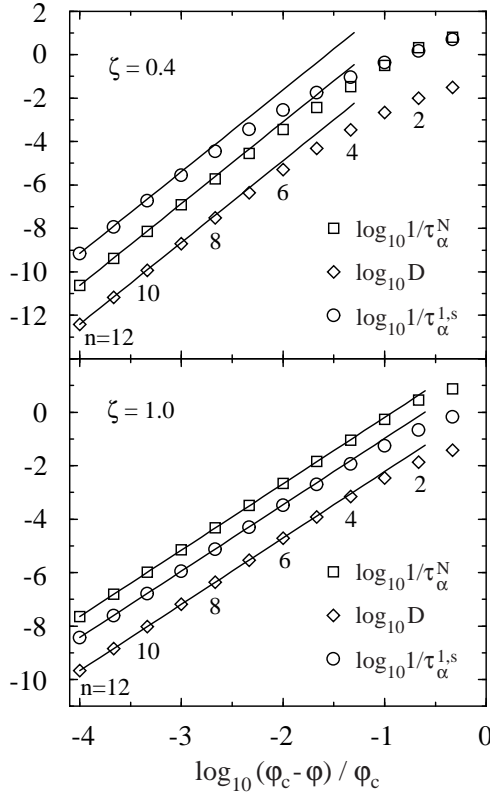


FIG. 12: Double logarithmic presentation of the relaxation rates $1=^N$ (squares) for the coherent total density correlator $h_q^N(t)$ at the structure-factor-peak position, $1=^{1;s}$ (circles) for the dipole correlator $C_{1;s}(t)$, and the diffusion coefficients D (diamonds) for the elongations $\zeta = 0.4$ (upper panel) and 1.0 (lower panel) as function of the reduced packing fraction $(\phi_c - \phi)/\phi_c = 10^{-n/3}$. The scaling times $1=^N$ and $1=^{1;s}$ are defined as in Eq. (19). The solid lines are the power-law asymptotes $A_j j$ (see text) with $\beta = 3.77$ and 2.48 for $\zeta = 0.4$ and 1.0 , respectively. The prefactors A have been chosen so that the solid lines go through the data points for $n = 12$.

by the convention given in Eq. (19).

Let us first consider the results for $\zeta = 1.0$. Although the asymptotic behavior is the same for all the quantities, $1=^{1;s}$ and D start to deviate visibly from their asymptotic results for $n = 4$, while $1=^N$ starts to deviate only for $n = 2$. The mentioned scale universality holds in the leading asymptotic limit for $\zeta \rightarrow 0$, and the corrections to the asymptotic predictions are different for different quantities. Thus, the found feature in the results for $\zeta = 1.0$ underlines the nonuniversality of the deviations. Let us add that the range of validity of the asymptotic-law description is quite similar to that of the hard-sphere system [2, 3]. The results for $\zeta = 1.0$ follow the pattern that has been analyzed theoretically so far. The results for $\zeta = 0.4$ exhibit much more pronounced deviations from the asymptotic-law predictions: $1=^N$ and D start to deviate visibly for $n = 7$, and the

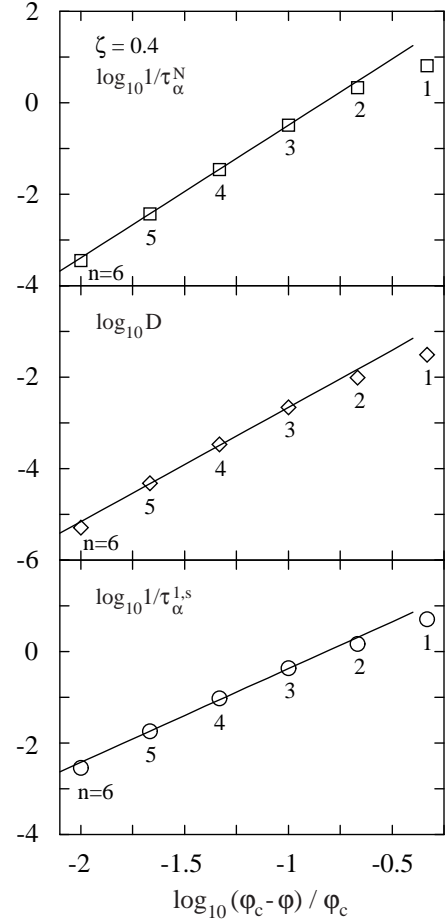


FIG. 13: Results as in Fig. 12, but only for a restricted region of the reduced packing fraction, $n = 6$, for the elongation $\zeta = 0.4$. The solid lines here are the power-laws $A_j j$ with the effective power-law exponents $\beta = 2.90, 2.50$, and 2.05 for $1=^N$, D , and $1=^{1;s}$, respectively. The prefactors A have been chosen so that the solid lines go through the data points for $n = 5$.

deviation of $1=^{1;s}$ starts even for $n = 9$. These deviations are due to the corrections to the scaling law. Their magnitudes are proportional to the product of the critical amplitudes for each quantity and the coefficient B_1 as noted in Eq. (26). The critical amplitude h_q^N for $\zeta = 0.4$ at the structure-factor-peak position is slightly larger than the corresponding result for $\zeta = 1.0$ (cf. Fig. 9 of Ref. 1). In addition, B_1 is 3.5 times larger for $\zeta = 0.4$ than for 1.0 . This is the reason for the larger deviation of $1=^N$ found for $\zeta = 0.4$ than the one for $\zeta = 1.0$, and similarly for D . The even more pronounced deviation for $1=^{1;s}$ is due to the large critical amplitude $h_{1;s}$ caused by the precursor effect of the nearby type-A transition, as discussed in connection with Fig. 13 of Ref. 1. Another possible source for the large deviations for $\zeta = 0.4$ might be due to higher-order glass transition singularities, which can lead to the violation of the second scaling law, and thus the scale universality. The signature

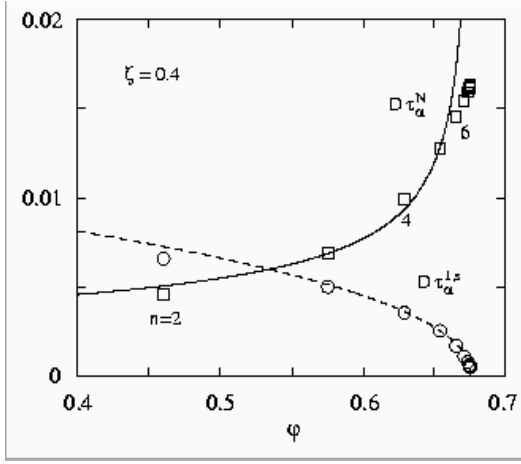


FIG. 14: Products D^N (squares) and $D^{1;s}$ (circles) for the τ -relaxation scales of the $\zeta = 0.4$ liquid shown in Figs. 12 and 13. The full (dashed) line is a power-law $\tau \propto j^{-\alpha}$ with α chosen so that the line goes through the data point for $n = 5$ and $\alpha = 0.40$ (0.45).

of such singularities is the approach of τ towards unity, which implies a divergency of B_1 .

A remark shall be added concerning the determination of the exponent entering the power-law behavior for the τ -relaxation time scale or relaxation rate as specified by Eq. (20). This result is based on the validity of the scaling law. Therefore, one cannot appeal to MCT if one tests power laws for τ -relaxation rates for cases where the scaling law is violated so strongly as shown in the upper panel of Fig. 7 for $x = 2$, i.e. for $n = 6$. Figure 13 demonstrates that, for $\zeta = 0.4$, the τ -relaxation rates for $j \propto 10^2$ can be fitted well by power laws $1 = j^{-\alpha}$ for an about 1.3-decade variation of the distance parameter j . The used effective exponent $\alpha = 2.90$ ($2.50; 2.05$) describes the variation of $1 = D^N$ ($D^{1;s}$) over 3.5 ($3.3; 2.5$) orders of magnitude. The variable-dependent effective exponent α again underlines the nonuniversality of the deviations from the scaling law. The quantities α are mere parameters without well-defined meaning for the discussion of our theory. They depend on the interval of j chosen for the fit.

Another manner for testing the coupling between the scales of two variables, say Y and Y^0 , is provided by a plot of the ratio $Y = Y^0$ versus the control parameter. Such a plot does not require the knowledge of τ_c , nor is it biased by the choice of some τ interval. This is demonstrated in Fig. 14 for the ratios formed with D^N or $D^{1;s}$ and the scale for the diffusivity $D / 1 = D$. Instead of weakly τ -dependent ratios expected for the asymptotic law, the figure shows variations by more than a factor 3. The shown plot suggests power-laws $Y = Y^0 / (\tau_c / \tau)^\alpha$ as shown by the full line with $\alpha = 0.40$ and the dashed one with $\alpha = 0.45$. The exponents α are the differences of the effective exponents α referring to Y and Y^0 .

IV. CONCLUSIONS

The recently developed mode-coupling theory (MCT) for molecular systems has been applied to calculate the standard correlation functions which demonstrate the evolution of glassy dynamics of a symmetric hard-dumbbell system (HDS). The equilibrium structure of this system is determined solely by excluded-volume effects, i.e., the sluggish dynamics and the structural arrest are due to steric hindrance for translational and reorientational motions. The phase diagram demonstrates that there are two scenarios for the liquid-glass-transition dynamics: one deals with strong and the other with weak steric hindrance for reorientational motion [1].

For the strong-steric-hindrance scenario, as it is obtained for dumbbells of elongation exceeding, say, 0.6, the constituent atoms are localized in cages of a similar size as found for the simple hard-sphere system (HSS) and for the motion of a single dumbbell in the HSS, Fig. 11. The parameter ζ , which determines the anomalous exponents of the decay laws and the critical time scales, is close to that of the HSS, Fig. 1. The range of validity of the scaling laws for the τ - and τ -processes, exemplified in the lower panels of Figs. 6 and 7, respectively, is similar to what was found for the HSS [2, 3] and for the motion of a hard dumbbell in the HSS [8, 11]. The rotation-translation coupling implies for the mean-squared displacement of the constituent atom a crossover interval between the end of the von Schweidler process and the beginning of the diffusion process which is about an order of magnitude larger than for the motion of a sphere in the HSS. This effect is even more pronounced for the dumbbell liquid, the lower panel of Fig. 10, than for a dumbbell moving in the HSS [11]. Testing this prediction by a molecular-dynamics simulation would provide a valuable information on the relevance of our theory.

The results of this paper together with the preceding findings on the τ -peaks for reorientational motion for angular-momentum index $\ell = 1$ and $\ell = 2$ as well as for the elastic modulus [8] lead to the conclusion that the strong-steric-hindrance scenario explains the qualitative features of the structural relaxation in glass-forming van der Waals systems like orthoterphenyl, Salol, or propylene carbonate. This holds with two reservations. First, the calculated wave-vector dependence of the Debye-Waller factor f_q^N is stronger than that measured by neutron-scattering spectroscopy for orthoterphenyl [12]. It remains to be shown that application of the theory to molecules more complicated than dumbbells will lead to a smearing out of the strong q -variations characteristic of hard-sphere-like systems. Second, molecules which allow for a measurement of the dipole-correlator by dielectric loss spectroscopy carry an electric dipole moment. This leads to long-ranged interactions between the molecules. It remains to be studied how the incorporation of these interactions change the results based solely on hard-core interactions.

The dipole-susceptibility spectra for a dumbbell with large α moving in a HSS [8] obey the scaling proposed by Dixon et al. [13]. We found this is the case also for the spectra of the HDS for elongations in the range $0.6 < \alpha < 0.8$. For $\alpha = 1.0$, on the other hand, the spectra for the high-frequency wing are below the master curve found in Ref. 13, and for $\alpha = 0.6$ they are slightly above. Thus, our theory is not consistent with the conjecture that the quoted scaling law holds universally.

Decreasing the elongation, the steric hindrance effects for reorientations weaken. A new scenario emerges for sufficiently small α for two reasons. First, there is a critical elongation α_c separating a normal glass from a plastic one. For $\alpha_A = (\alpha_c) = \alpha_c$ approaching zero, the critical amplitudes $h_{q;s}^z$, in particular $h_{1;s}^z = \lim_{q \rightarrow 0} h_{q;s}^z$, diverge. This transition is due to the top-down symmetry of the molecules. But the asymptotic formulas for small α remain valid also for nearly symmetric molecules; one merely has to replace j_A by $\frac{1}{\alpha^2 + 1}$, where α is a number quantifying the symmetry breaking [14, 15]. The precursor phenomena of the approach of α_c towards α_c have been discussed before for the motion of a single dumbbell in a HSS [8]. The most obvious one is the speeding up of the α -process for reorientations relative to that for density fluctuations, as demonstrated in Fig. 2. The second reason is the strong increase of the exponent parameter for α_c , Fig. 1. For $\alpha = 1$, there occurs a higher-order glass transition singularity, where the asymptotic expansions of the MCT solutions are utterly different from those cited in Sec. IIB. The approach of towards unity leads to a shrinking of the range of validity of the discussed universal formulas. The corrections diverge, as was discussed in connection with the coefficient B_1 in Eq. (26). This equation shows that the increase of the product $B_1 h_{1;s}^z$ leads to an increasing violation of the superposition principle for the α -process, as shown in the upper panel of Fig. 7. As a result, the α -relaxation time approaches the universal law, Eq. (20), only for very small distance parameters $\alpha = (\alpha_c - \alpha) = \alpha_c$. For $\alpha = 1.0$, the power-law regime is reached for $j = 10^1$, while j has to be smaller than 10^2 for the approach to the asymptotic law for $\alpha = 0.4$, Fig. 12. A decrease of j by an order of magnitude is equivalent to an increase of the relaxation time by more than a factor of 1000.

For $\alpha = 0.4$, the variation of the α -relaxation-time scales over more than three orders of magnitude can be described well by power laws, Fig. 13. But, the above-explained corrections to the leading-order asymptotic laws imply that the fitted effective exponents α_e are considerably smaller than the exponent $\alpha = 3.77$ specifying the correct asymptotic behavior. Moreover, the corrections depend on the variable considered and therefore the found effective exponents are pairwise different. This means that the α -relaxation scales are not coupled, rather the ratio of two scales varies according to a power law as shown for two cases in Fig. 14. Molecular-dynamics-simulation studies for a binary Lennard-Jones system which have been started by Kob and Ander-

sen [16] have been used for detailed tests of MCT, as can be inferred from Ref. 17 and the papers cited there. The range of time variations for the α -process in these studies is about the one considered in Fig. 13. As a remarkable deviation from the α -scale universality, a deviation of the α -exponent for the diffusivity from the exponent derived from density-relaxation curves has been reported [16]. Indeed, the D - α -diagram for the simulation data is in semi-quantitative agreement with the results shown in Fig. 14 [18]. Therefore, it is tempting to conjecture that the simulation data can be explained as done above for the results in Figs. 13 and 14.

We are not aware of experiments which exhibit the weak steric hindrance scenario. Molecular-dynamics simulations for a liquid of symmetric Lennard-Jones dumbbells with elongation $\alpha = 0.33$ lead to the suggestion [19] that an inclusion of the rotational degrees of freedom is decisive for an understanding of the exponent parameter. This conclusion is corroborated by Fig. 1. Detailed simulation studies of the glassy dynamics of a liquid of slightly asymmetric Lennard-Jones dumbbells for $\alpha = 0.5$ have been reported by Kammerer et al. [20, 21, 22]. The correlation functions dealing with the translational degrees of freedom for large and intermediate wave vectors and also the ones for reorientational fluctuations for large angular-momentum indices could be interpreted with the universal MCT formulas. However, the dipole correlator did not show a two-step-relaxation scenario and it exhibited strong violations of the superposition principle quite similar to what is shown in the upper panel of Fig. 7. The α -relaxation time scales for density fluctuations of intermediate wave vectors, for the diffusivity, and for the dipole correlator could be fitted well by power laws with the exponents 2.56, 2.20, and 1.66, respectively. The differences in these exponents are quite similar to what is demonstrated in Fig. 13 for the corresponding quantities. This explains why the D - α (versus temperature) diagram for the simulation results [23] shows violations of the scale coupling in semi-quantitative agreement with the ones shown in Fig. 14. It seems that the simulation results for $C_{1;s}(t)$ also fit nicely into the framework of the ideal MCT for molecular liquids.

Let us notice that the density correlators of the glass states for wave vector $q = 9.8$ exhibit oscillations for times around 0.1, Figs. 2 and 3. These are the analogues of the oscillations analyzed previously for the HSS in connection with a discussion of the so-called boson-peak phenomenon and high-frequency sound [24]. It should be mentioned that the dynamics of a dipolar-hard-sphere system was analyzed recently within the mode-coupling theory [25] describing the structure by tensor-density fluctuations. Some comments on the general relation between this theory and the one used in the present paper can be found in Refs. 1 and 25. For the dipolar-hard-sphere system, the oscillations have been analyzed in detail. They reflect subtle couplings between translational and rotational degrees of freedom as enforced by the long-ranged Coulomb interactions. For the HDS such

couplings are present as well, albeit caused by the short-ranged steric hindrance effects; but an analysis of these oscillations remains to be done.

Acknowledgments

We thank W. Kob cordially for discussions and suggestions. We thank him as well as M. Sperl, Th. Voigtman,

and R. Schilling for helpful critique of the manuscript.

-
- [1] S.-H. Chong and W. Gotze, Phys. Rev. E, in press; also at cond-mat/0112127.
 - [2] T. Franosch, M. Fuchs, W. Gotze, M. R. Mayr, and A. P. Singh, Phys. Rev. E 55, 7153 (1997).
 - [3] M. Fuchs, W. Gotze, and M. R. Mayr, Phys. Rev. E 58, 3384 (1998).
 - [4] J. P. Hansen and I. R. McDonald, Theory of Simple Liquids, 2nd ed. (Academic Press, London, 1986).
 - [5] D. Chandler and H. C. Andersen, J. Chem. Phys. 57, 1930 (1972).
 - [6] L. J. Lowden and D. Chandler, J. Chem. Phys. 59, 6587 (1973).
 - [7] W. Gotze, J. Phys.: Condens. Matter 2, 8485 (1990).
 - [8] S.-H. Chong, W. Gotze, and A. P. Singh, Phys. Rev. E 63, 011206 (2001).
 - [9] E. O. Tuck, Math. Comp. 21, 239 (1967).
 - [10] W. Gotze, J. Stat. Phys. 83, 1183 (1996).
 - [11] S.-H. Chong, W. Gotze, and M. R. Mayr, Phys. Rev. E 64, 011503 (2001).
 - [12] A. Tolle, J. Wuttke, H. Schober, O. G. Randl, and F. Fujara, Eur. Phys. J. B 5, 231 (1998), and references quoted there.
 - [13] P. K. Dixon, L. Wu, S. R. Nagel, B. D. Williams, and J. P. Carini, Phys. Rev. Lett. 65, 1108 (1990).
 - [14] T. Franosch and W. Gotze, J. Phys.: Condens. Matter 6, 4807 (1994).
 - [15] T. Franosch and A. P. Singh, J. Non-Cryst. Solids 235 (237), 153 (1998).
 - [16] W. Kob and H. C. Andersen, Phys. Rev. Lett. 73, 1376 (1994).
 - [17] W. Kob, J. Phys.: Condensed Matter 11, R85 (1999).
 - [18] W. Kob, private communication (1999).
 - [19] W. J. Ma and S. K. Lai, Phys. Rev. E 55, 2026 (1997).
 - [20] S. Kammerer, W. Kob, and R. Schilling, Phys. Rev. E 56, 5450 (1997).
 - [21] S. Kammerer, W. Kob, and R. Schilling, Phys. Rev. E 58, 2131 (1998).
 - [22] S. Kammerer, W. Kob, and R. Schilling, Phys. Rev. E 58, 2141 (1998).
 - [23] A. Latz and R. Schilling, private communication (1998).
 - [24] W. Gotze and M. R. Mayr, Phys. Rev. E 61, 587 (2000).
 - [25] T. Theenhaus, R. Schilling, A. Latz, and M. Letz, Phys. Rev. E 64, 051505 (2001).